Laser vibrometry characterisation of a microfluidic lab-on-a-chip device: a preliminary investigation

Article (Published Version)

Laser vibrometry characterisation of a microfluidic lab-on-a-chip device: a preliminary investigation

Journal of Physics: Conference Series **498** (2014) 012002 doi:10.1088/1742-6596/498/1/012002

Laser vibrometry characterisation of a microfluidic lab-on-a-chip device: a preliminary investigation

C Fury[1,2], P N Gélat[2,3], P H Jones[1] and G Memoli[2]

[1] Department of Physics and Astronomy, University College London, Gower Street, London, WC1E 6BT, UK

[2] National Physical Laboratory, Teddington, Middlesex, TW11 0LW, UK

[3] Department of Mechanical Engineering, University College London, Torrington Place, London, WC1E 7JE, UK

Since their original inception as ultrasound contrast agents, potential applications of microbubbles have evolved to encompass molecular imaging and targeted drug delivery. As these areas develop, so does the need to understand the mechanisms behind the interaction of microbubbles both with biological tissue and with other microbubbles. There is therefore a metrological requirement to develop a controlled environment in which to study these processes. Presented here is the design and characterisation of such a system, which consists of a microfluidic chip, specifically developed for manipulating microbubbles using both optical and acoustic trapping. A laser vibrometer is used to observe the coupling of acoustic energy into the chip from a piezoelectric transducer bonded to the surface. Measurement of the velocity of surface waves on the chip is investigated as a potential method for inferring the nature of the acoustic fields excited within the liquid medium of the device. Comparison of measured surface wavelengths with wave types suggests the observation of anti-symmetric Lamb or Love-Kirchhoff waves. Further visual confirmation of the acoustic fields through bubble aggregation highlights differences between the model and experimental results in predicting the position of acoustic pressure nodes in relation to excitation frequency.

1. Introduction

The biomedical application of microbubbles has been documented back to the 1960s [1]. But only in the last decades has the technology been developed to manufacture gas bubbles safe enough to inject into the human body. Bubbles with a radius in the range 2-8μm have a resonant volume oscillation excitation in reaction to MHz ultrasound, an effect which reradiates the impinging sound back out into the medium at a higher region of the frequency spectrum [2]. The resulting scattered field is highly responsive to the nature of the incoming ultrasound. As this frequency range is suited to the medical ultrasound scanner frequencies it has led to an increasing interest in microbubble use as biomedical sensors, contrast agents for ultrasound imaging and potentially as drug delivery vehicles [3]. As the sophistication of these applications increases, it is likely that the accurate modelling and understanding of how different bubble compositions respond to ultrasound will become increasingly important in ensuring the safety and efficacy of new products. There is therefore a requirement to develop a controlled environment in which to study the metrological aspects of the interactions between bubbles and sound fields.

Many studies have investigated the response of bubbles to sound fields. Early research into the acoustic emissions from cavitating bubbles [4] drew conclusions from large populations. It has been shown however that if bubbles are sufficiently close to one another they will interact [5] and this will in turn affect the emitted sound field. This indicates that it may be difficult to understand single bubble behaviour from experiments on bubble populations.

More recently, techniques have arisen to manipulate single bubbles to investigate their acoustic response in isolation [6][7]. These include techniques using kHz frequency acoustic fields which allow the position of bubbles in suspension to be controlled [7]. Using standing wave fields, the same technique may be used to trap bubbles at pressure nodes. The ability of this technique to manipulate many bubbles simultaneously makes it a potentially powerful tool for bubble characterisation by providing a facility which moves out of the large population regime.

The aim of this study is to characterise a custom lab-on-a-chip device designed for confining and measuring the response of microbubbles to MHz frequencies under controlled isolation. The microfluidic chip was designed and modelled using finite element modelling (FEM) at the National Physical Laboratory (NPL) and fabricated by Dolomite Microfluidics Ltd. We also discuss a scanning laser vibrometer method for characterising the acoustic fields excited within the chip. A similar technique has been employed by Neild *et al.*[8] in which a vibrometer is used to directly observe the vibration of a line upon a piezoelectric element in order to search for resonant excitation frequencies.

Here, this technique is extended to observe an entire driven surface near and far (up to 3 wavelengths) from a driving piezo element, to investigate standing waves in the excited structure that may suggest suitable frequencies for the acoustic trapping of particles. Comparison of the results with FEM allows verification and improvement of simulations.

The ability to accurately simulate what is happening inside the microfluidic channel will ultimately facilitate predictions of the pressure within the fluid. This cannot be measured directly experimentally as the introduction of a hydrophone with a size comparable to the channel would disrupt the acoustic field, significantly modifying the acoustic pressure values observed.

2. Microfluidic chips and experimental set up

The microfluidic chips used here have been designed to accommodate acoustic trapping, ultrasonic bubble excitation and optical tweezing. Simulations of resonant bubble motion [9] have shown that the bubbles will require a trapping force in the 1-10 nN range to maintain a stable trapped position. This magnitude of force cannot be produced by optical trapping alone and so must be complemented by acoustic trapping. The combined two tweezer system combines the relatively large acoustic trapping force with the high spatial resolution provided by optical tweezing.

The microchannel that contains the bubbles is labelled (1) in figure 1. The channel has four tubes that converge at the centre of the chip and are fed from the outer left and right edges. The straight portion at the bottom edge will be referred to as the ‘main channel’ and is the focus of the work described here. The diagonal channels are referred to as the left and right ‘legs’. Pressure waves in the liquid contained in the channel are excited by a PZT (Lead zirconium titanate piezoelectric ceramic) transducer attached to the surface of the chip.

The microfluidic chip (maximum thickness 2.54 mm (in the central section containing the microchannel) and minimum thickness 1.2 mm (where the inlet ports are mounted)) was filled using a software controlled syringe pump (Kloehn, model 54022) and then sealed, so preventing the leakage of any fluid during use.

The cuboid in figure 1 (5.9 x 5.9 x 13 mm) is a PZT4 piezo transducer (Morgan Ceramics, UK) and its driving signal was generated with an Agilent 33250A signal generator providing 40mV_{pp} amplitude, amplified by an A&I 250L and impedance matched with a 1:25 toroidal transformer.

The laser vibrometer (Polytec Ltd., PSV-400) was used to scan the top surface of the microfluidic chip and record its velocity in the normal direction to the microchip surface during operation. The internal software synchronises the velocity data at each scanning point to the signal driving the PZT, obtaining the temporal evolution of the surface and its root mean squared velocity. In the set up used

for this study, the device was triggered by the TTL output from the Agilent generator so that it is directly coupled to the PZT action.

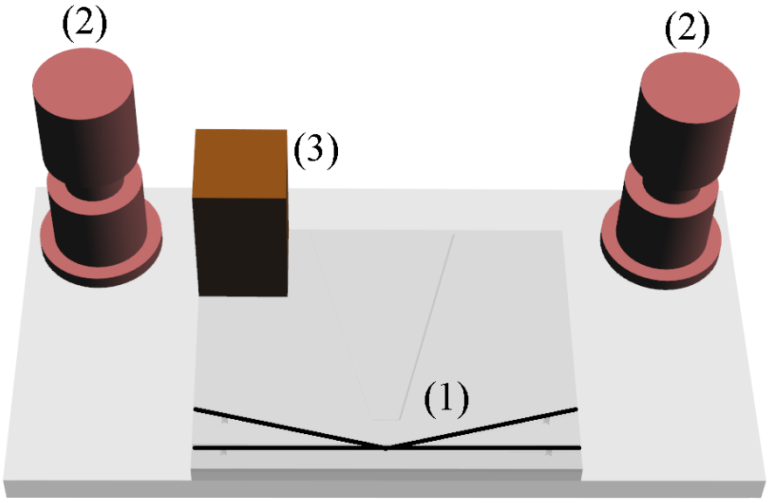

Figure 1. Microfluidic chip for optical and acoustic tweezing. The microchannel is visible at the lower edge of the chip in the form of a 'K' rotated 90° counter-clockwise (1). The cylindrical structures depict the fluidic in/out ports (2) and the cuboid is the PZT transducer used to drive the surface (3).

3. Modelling

In order gain a better understanding of the piezoelectric, mechanical and acoustical interactions between the driving transducer and the glass microfluidic chip, FEM simulations were carried out using the PAFEC VibroAcoustics software [10]. The model represents a 25 mm × 20 mm × 2.5 mm cuboid glass chip with water inlet holes and microchannels, together with a sinusoidally-driven cuboid piezo-ceramic transducer, as described in Section 2.

The mesh was generated using CATIA v5 Advanced Meshing Tools. Ten-noded tetrahedral elements with quadratic shape functions were used throughout the mesh, with a maximum separation of adjacent corner nodes of 1.5 mm in each element. For quadratic elements, it is well known that it is generally sufficient to mesh at three elements per wavelength. At 180 kHz, the employed mesh density corresponds to a lowest wave speed of 810 m s^{-1} indicating that the mesh density is likely to be higher than required for the materials used. The glass elements possess three translational degrees of freedom in the *x*, *y* and *z* direction of the global Cartesian axis set. The fluid elements have a single degree of freedom (acoustic pressure) and are coupled to the structural elements via continuity of the normal component of the particle velocity vector at the structure/fluid interfaces. The coupling of the tangential component of the velocity is neglected in this analysis.

Ambient temperature conditions of 25 °C were assumed. The physical properties of water were calculated using temperature dependencies obtained from the literature [11] and those for glass were initially taken from online databases [12][13]. These properties attained from databases are detailed in Table 1.

Table 1: Properties of glass and water.

	Density kg m^{-3}	Young's Modulus GPa	Longitudinal speed of sound m s^{-1}	Poisson's ratio
Glass [12][13]	2234	8.01	6694	0.27
Water [11]	997.9	Not applicable	1488	Not applicable

The piezoelectric elements were defined in terms of their full orthotropic, piezoelectric and dielectric properties, as defined in the PAFEC modelling system [10]. These elements possess four degrees of freedom: *x*, *y* and *z* translations in the global Cartesian axis set along with electrical potential.

The fluid boundary conditions at the inlets and outlets were assumed to be zero normal pressure gradients. Translations along the *z*-axis were restrained at the base of the chip. The electrical degrees of freedom were restrained across the bonded bottom electrode (earth electrode condition) and a sinusoidal electrical excitation of 1 V magnitude was applied at all nodes on the top electrode (live electrode). The frequency of excitation was varied between 130 kHz and 180 kHz in 0.5 kHz steps. At each frequency, the FEM calculations enabled the structural displacement vectors, acoustic pressures and electrical potentials to be obtained.

4. Excitation frequency determination

Two drawbacks of using the laser vibrometer were that the instrument could only be employed for a single frequency at a time and, with the present software, a frequency sweep cannot be automated. Therefore suitable frequencies needed to be chosen beforehand in order to efficiently investigate the regions of interest. The FEM data can be used to predict at which frequencies modes of the structure will occur by summing the pressure throughout the channel for each simulation frequency. Peaks in the spectrum of this "spatially averaged pressure" (figure 2a) will correspond to resonant modes of the channel and are therefore optimal candidates for acoustical manipulation experiments. The FEM model indicates these to be located at 135, 139, 172.5, 173 and 179 kHz.

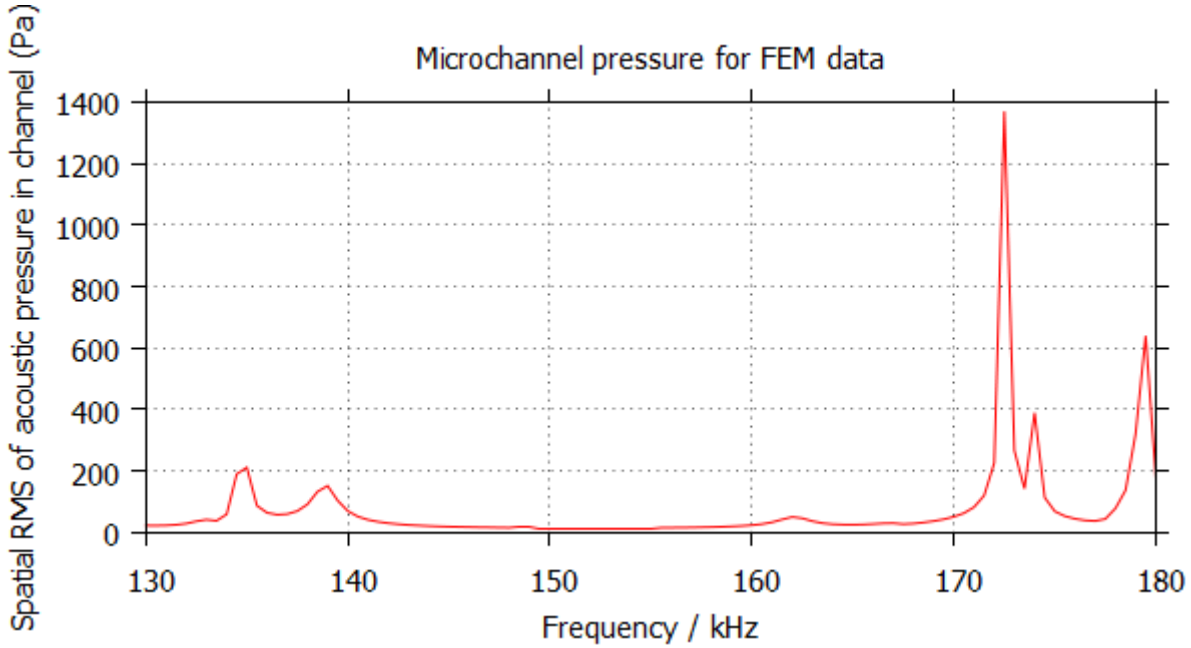

a)

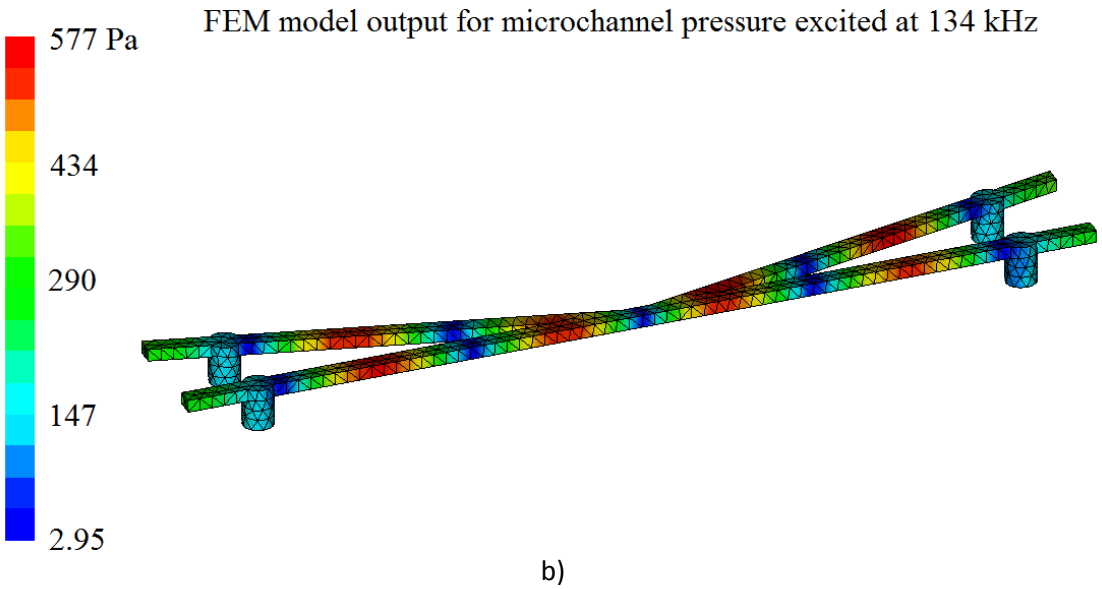

Figure 2. Spatially averaged RMS of the acoustic pressure in the microchannel for frequencies in the range 130-180 kHz (in 0.5 kHz steps) derived from FEM simulations. Peaks denote regions where increased pressure is seen in the channel and are likely to indicate a trapping frequency. The inset model (b) shows a uniform standing wave pattern is predicted in the channel at 134 kHz.

The uncertainty as to whether the material properties reported in table 1 are relevant to this particular glass specimen and the simplifications in the FEM model are reflected in the ambiguity of the resonance positions in the spectrum of figure 2; while the order (and the relative position) of the peaks is potentially correct, their frequency may appear different in practice. To directly test the chip for excitation an electrical impedance scan was performed to investigate resonances [14]. The results can be seen in figure 3, where resonances appear as peaks in the Real Impedance data and from which two frequencies were decided upon for the preliminary tests described later within this paper: 104 kHz and 162 kHz.

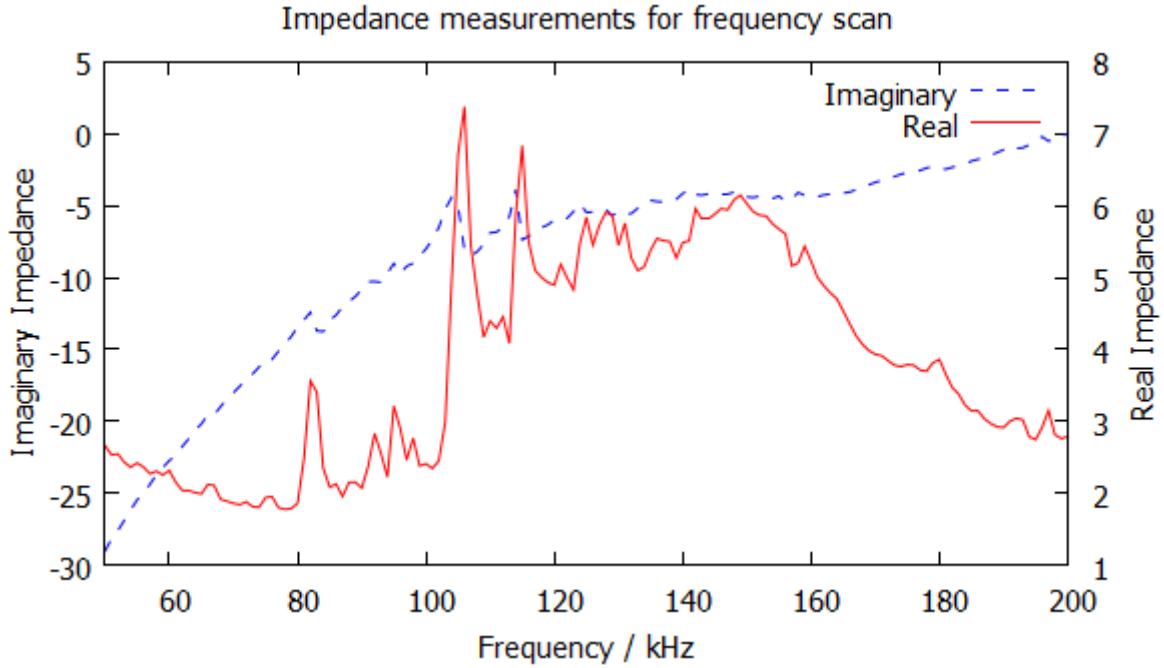

Figure 3. Electrical impedance data for the surface mounted transducer. Resonant frequencies occur for when there is a peak in the Real data and a negative slope in the Imaginary data.

5. Results

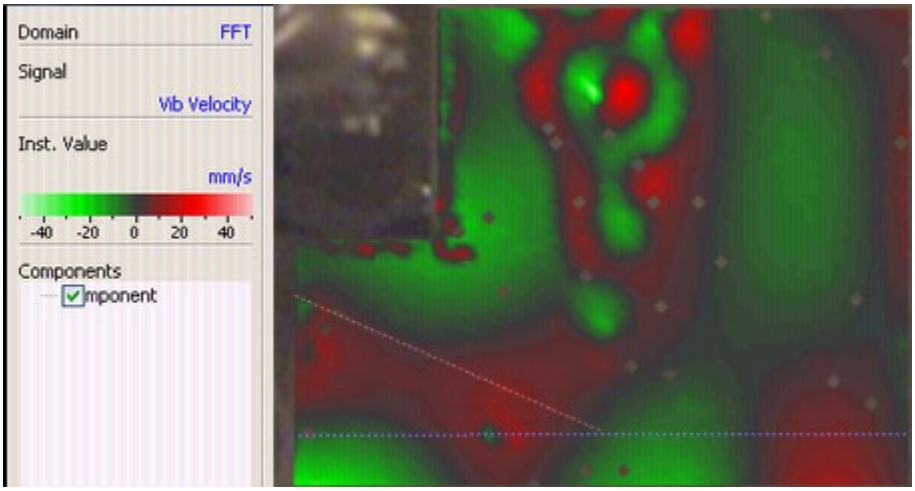

Figure 4. A sample of laser vibrometer data for a point in time during the driving frequency cycle at 162 kHz. The colour depiction denotes instantaneous velocity at each of the ~4500 data points in this scan.

Figure 4 shows an example data set from the vibrometer, with the colour scale representing the surface velocity at a point in time during the driving frequency cycle. The main channel has been identified as being located along the horizontal dashed line and the left leg along the diagonal line. Figure 5 shows a profile plot for the main channel at several evenly spaced phases in the driving oscillation cycle for 104 kHz. The position of the peak is denoted by the arrow and can be seen to be travelling to the right. For stable particle manipulation a standing wave must be observed and therefore this frequency is not a useful one. However, it should be noted that the magnitude of the velocity is high, likely suggesting that a structural mode is being excited.

Figure 6 shows similar information for a 162 kHz driving signal. Here the arrow marking the wave peak does not move in time, indicating a standing wave, this time with only an instantaneous velocity normal to the surface of one quarter of the magnitude of the 104k Hz case. A useful confirmation that the profile actually describes what is happening on the top of the microchannel can be seen in the data near the left-hand anti-node; there is a small region that appears to be oscillating 180° out of phase with the area around it. A post-scan inspection of the channel showed an air void within the liquid at this point. At a pressure free interface such as this we would expect a 180° phase change in the wave.

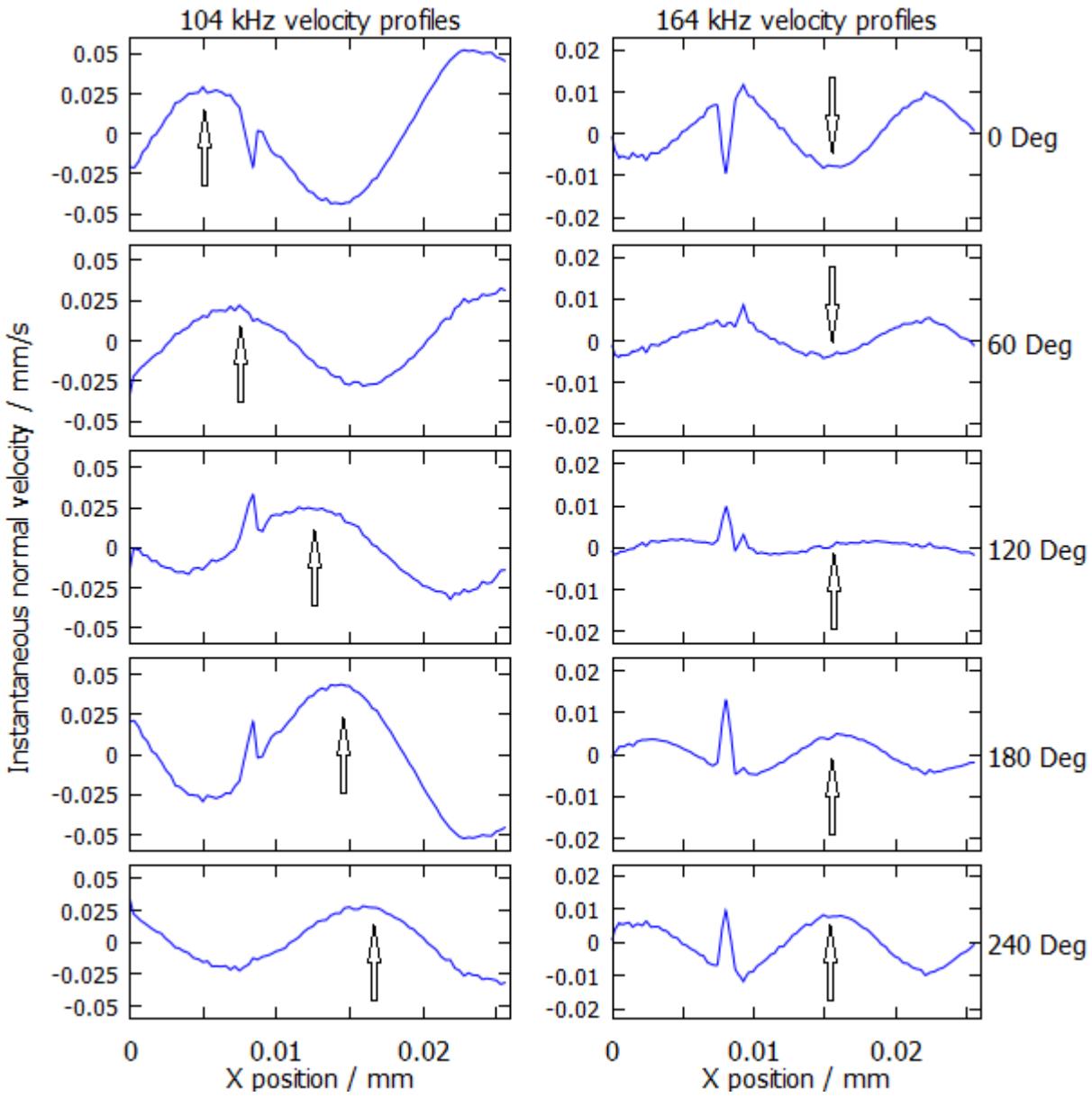

Figure 5. Normal velocity above the main microchannel for a 104 kHz excitation (vibrometer data). The wave observed is travelling to the right and will not provide suitable conditions for trapping. The arrow shows the movement of the wave peak.

Figure 6. Normal velocity above the main microchannel for a 162 kHz excitation (vibrometer data). A standing wave can be seen with the peak denoted by the arrow. An air void shows a 180° phase change in wave velocity at the left hand antinode.

To prove that close to 162 kHz it is possible to aggregate particles, Expancel microspheres (AkzoNobel, 461-WU-40 polymer microspheres, 12-16 μm diameter) were pumped into the channel and a microscope used to capture their movement while the chip was excited through the PZT. After 20 seconds, grouped spheres could be observed (see figure 7), while no aggregation was observed at 104 kHz. Due to the size of the Expancel the clusters form at nodes in the field [15][16] and this can be used to measure the half wavelength of the standing wave. Figure 7 reports one of those values by the overlaid arrow, averaging between all visible nodal points gives a longitudinal wavelength in water

of 8.9 ± 0.4 mm, which is comparable with the expected value of 9.3 mm (calculated using the speed of sound in water [11] and a driving frequency of 163.4 kHz). This node-node distance and the arrangement of nodes across the chip mirrors a state predicted by the FEM, given in figure 2b. The similarities are stark, but the two examples are performed at different frequencies with the experiment at 163.4 kHz and the model at 134 kHz. This raises a question over whether the model is complete enough (e.g. currently the damping terms are neglected) or if the tabulated data that was used to define the materials is incorrect.

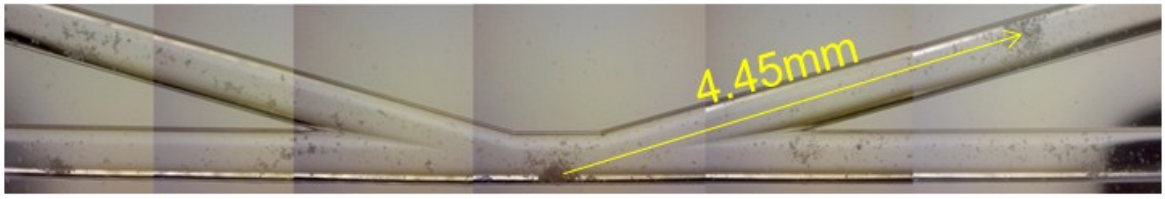

Figure 7. Composite image taken after aggregation of Expancel microspheres in a 163.4 kHz acoustic field. The distance between aggregation sites is λ/2 and the theoretical longitudinal wavelength in water agrees with the measured value of 8.9 mm. The Image was calibrated using a NPL graticule, with a resolution of 25 μm.

6. Discussion

In the previous section, we presented a comparison between wavelengths measured from the images of bubble aggregation and the ones predicted by the FEM model, finding that:

a. at 163.4 kHz, where aggregation and a standing wave have been observed, the pressure wave wavelength agrees with the theoretical one in water;
b. at 134 kHz the pressure wave wavelength predicted by the FEM agrees with that measured at 163.4 kHz, supporting a similar layout of the acoustic field; but not the theoretical wavelength in water at this frequency (11.2 mm).

As previously mentioned the reason for matching FEM modelling with experiments is related to the problem of measuring pressure in the microchannel. The laser vibrometer was able to determine whether a standing wave was present at the surface, but it was not clear whether it could it be used to infer the pressure distribution inside the channel.

Snell's law [17] predicts that at the interface between two different media (glass and water, in this case) the ratio of wavelengths is equal to the ratio of wave speeds in the two different media. Knowing the speed of sound and the measured wavelength in water, the corresponding values in glass and the type of wave that has been measured on the chip surface are needed.

The laser vibrometer was used to capture the wavelength of the surface wave at the top of the chip, giving a value of 13.3 ± 1 mm (figure 6), corresponding to a measured wave speed of 2154 ±160 m s^{-1} for a 162 kHz driving frequency. The first logical comparison is with the speed of shear waves, which can be obtained using the following equation [18]:

$$c_s = \left[\frac{E}{2(1+\nu)\rho}\right]^{1/2} \quad (1)$$

Where c_S is the shear wave speed, E the Young's modulus, ν is Poisson's ratio and ρ is the density.

Equation 1 and the values in table 1 give a shear wave speed of 3330 m s^{-1}, which is much higher than that measured. There were two likely reasons for this which are explored below.

The first was that the material data for the glass in table 1 was incorrect. Consequently the longitudinal wave speed in the glass was measured using a pulse-echo technique at 5600 ± 60 m s^{-1} (1 s.d.) and the density at 2594 ± 30 kg m^{-3} (1 s.d.); both values lie close to the tabulated ones. The Poisson ratio and the Young's Modulus of glass sit within a narrow band [15] and cause only a small change to the velocity result. Taking the mean values from tabulated data [12][13] (0.219 for the Poisson's ratio and 7.14×10^{10} Pa for the Young's modulus) produces a shear speed result of 3360 ms^{-1},

very similar to the one obtained from tabulated data and not significantly closer to the measured wave speed. Even if in future studies these unknown material properties will be measured, another wave description must be found in order to bridge the gap between experiment and current theory.

The second possibility is that the treatment of these waves as shear waves has been too simple and that a more involved wave model is needed. The waves we considered were Rayleigh, Lamb and Love-Kirchhoff waves, with the closest result being shared between the Lamb and Love-Kirchhoff regimes.

The Lamb wave is an elastic wave that establishes in a vibrating, free plate, of infinite planar size, and where the wave velocity is governed by a finite plate thickness. The thickness of the microchip being 2.5 mm, this would give a wave speed (Rose [19], P. 111 Equation 8.39) of 1757 m s^{-1}. The Love-Kirchhoff wave is similarly an elastic wave that propagates in a free plate but of both finite planar dimensions and thickness and governed by the 2D modes being excited. This gives an expected speed of 2299 m s^{-1}, using x = 4^{th} mode y = 2^{nd} mode as seen in figure 4. This is higher than observed by one standard deviation; closer than the Lamb wave which is lower by twice the standard deviation.

In particular, this study has only used 2 frequencies for the vibrometer, of which only one was found to be viable for trapping and comparisons. Future studies will include more frequencies and successfully pick appropriate trapping frequencies from the impedance data to compare against FEM results across the entire spectrum. Both the Lamb and Love-Kirchhoff waves are dispersive to different degrees. A wider investigation of excitation frequencies will show a tendency to favour one dispersion curve over the other and so deliver the correct wave type.

With a larger database, similarities or offsets in the real compared to FE-modelled frequencies may appear that can then be treated for by different effects such as damping. In the short term experimental work can be progressed by factoring out any offsets in the correct positions of the modelled frequencies to produce a more efficient trapping frequency predicting technique. Once a quantifiable shift or scaling of the frequencies can be found, we may begin to understand the causes of the disparity seen and update the model further.

7. Conclusions

This work presents the results of a preliminary study into the characterisation of surface waves upon a microfluidic chip that is intended for acoustic microbubble manipulation. A laser vibrometry technique was employed to measure surface normal velocities upon a chip excited at different frequencies. The technique was used successfully to detect standing waves upon the chip surface at a frequency that was also seen to generate a standing wave within the microfluidic channel inside of the chip; enabling the identification of frequencies suitable for acoustic trapping.

The technique was also shown to be able to detect air voids within the liquid, raising confidence in that it can be used to directly measure what is happening in the liquid even though it is imaging the glass surface above it. The ability to both observe the glass wave motion and infer the pressure distribution within the microchannel enable the data gained to be directly compared to finite element modelling of the chips.

So far the surface wave results have been unexpected and differ from modelling predictions. The surface velocities lay in a region between those expected for anti-symmetric Lamb waves and Love-Kirchhoff waves, with these being lower and higher respectively. Further work must be carried out to obtain the correct material properties for the glass so that the validity of the speeds from equation 1 and table 2 can be verified.

Additionally, the number of frequencies explored through the laser vibrometer will be increased to enable a more complete comparison with the FEM, underpinning an understanding of the frequency shift and allowing models to be adjusted. When the models produce a result comparable to observations they can begin to be used as a tool to interrogate the pressures involved in the acoustic manipulation, a measurement that is difficult to obtain in practice.

Acknowledgements

The authors acknowledge funding from EPSRC and the National Physical Laboratory Strategic Research programme. Useful discussions with C Harfield and E J Stride, University of Oxford, and B Zeqiri, NPL, are also gratefully acknowledged.

References

[1] Kremkau F W, Gramiak R, Shah P M, Carstensen E L and Kramer D H, 1970, "Ultrasonic detection of cavitation at catheter tips", *Am. J. of Roentgenology, Radium Therapy, and Nuclear Medicine*, 110 (1):177.

[2] Zeqiri B, Gelat, P N, Hodnett M and Lee N D, 2003, "A novel sensor for monitoring acoustic cavitation. Part I: Concept, theory, and prototype development," *Ultrasonics, Ferroelectrics and Frequency Control, IEEE Transactions on*, **50** (10), 1342-50.

[3] Blomley M J K, Cooke J C, Unger E C, Monaghan M J, and Cosgrove D O, 2001, "Microbubble contrast agents: a new era in ultrasound", *BMJ*, **322**.

[4] Neppiras E A, 1968, "Measurement of acoustic cavitation", *IEEE transactions on Sonics and Ultrasonics*,SU-**15** (2), 81-88.

[5] Garbin V, Ferrari E, Cojoc D, Fabrizio E, Overvelde M L J, Van der Meer S M, Versluis M, De Jong N and Lohse D, 2006, "Optical Trapping of Ultrasound Contrast Agent Microbubbles: Study of the Bubble-Wall and Bubble-Bubble Interaction in Ultrasound," *Ultrasonics Symposium 2006. IEEE*, 513-16.

[6] P Jones, E Stride and N Saffari, 2006, "Trapping and manipulation of microscopic bubbles with a scanning optical tweezer", *Appl. Phys. Lett.* **89**, 081113.

[7] Rabaud D, Thibault P, Raven J-P, Hugon O, Lacot E, and Marmottant P, 2011, "Manipulation of confined bubbles in a thin microchannel: Drag and acoustic bjerknes forces", *Physics of Fluids*, **23**.

[8] Neild A, Oberti S and Dual J, 2007, "Design, modeling and characterization of microfluidic devices for ultrasonic manipulation", *Sensors and Actuators B*, **121**, 452-61.

[9] Harfield C, Pawlikowska A, Stride E, Jones P H and Memoli G, 2011, "Opto-acoustic trapping of microbubbles", Poster presented at the *Microbubble symposium: Fabrication, characterisation and translational applications*, Leeds, UK.

[10] PACSYS, PAFEC tool, 2010, www.vibroacoustics.co.uk.

[11] Bilaniuk N and Wong G S K, 1993, "Speed of sound in pure water as a function of temperature", *J. Acoust. Soc. Am.*, **93**, 1609-12.

[12] Tables of Physical & Chemical Constants (16th edition 1995). 2.1.4 Hygrometry. Kaye & Laby Online. Version 1.0 (2005).

[13] Schott B270 glass technical sheet, http://www.pgo-online.com/intl/katalog/B270.html , last accessed 04/04/2013.

[14] Barsoukov E and Macdonald J R, 2005, "Impedance Spectroscopy Theory, Experiment and Applications", 2nd Edition, New jersey, USA (Wiley).

[15] Lenshof A, Magnusson C and Laurell T, 2012, "Acoustofluidics 8: Applications of acoustophoresis in continuous flow microsystems", *Lab Chip*, **12**, 1210.

[16] Leighton T G, 1997, "The Acoustic Bubble", London (Academic Press).

[17] Gedge M and Hill M, 2012, "Acoustofluidics 17: Theory and applications of surface acoustic wave devices for particle manipulation", *Lab Chip*, **12**, 2998–3007.

[18] Pierce A D, 1989, "Acoustics: An Introduction to Its Physical Principles and Applications", Woodbury, NY (Acoustical Society of America), P. 130, Eq. 3-6.1.

[19] Rose J L, 2004, "Ultrasonic Waves in Solid Media", (Cambridge University Press), p. 111.